# Spin Vortex Crystal Order in Organic Triangular Lattice Compound

Kira Riedl,[1] Elena Gati,[2,3] David Zielke,[2] Steffi Hartmann,[2] Oleg M. Vyaselev,[4] Nataliya D. Kushch,[5] Harald O. Jeschke,[6] Michael Lang,[2] Roser Valentí,[1] Mark V. Kartsovnik,[7] and Stephen M. Winter[8,*]

[1]*Institut für Theoretische Physik, Goethe-Universität Frankfurt, Max-von-Laue-Strasse 1, 60438 Frankfurt am Main, Germany*
[2]*Physikalisches Institut, Goethe-Universität Frankfurt, Max von Laue Str 1, 60438 Frankfurt am Main, Germany*
[3]*Max Planck Institute for Chemical Physics of Solids, 01187 Dresden, Germany*
[4]*Institute of Solid State Physics, Russian Academy of Sciences, 142432 Chernogolovka, Russia*
[5]*Institute of Problems of Chemical Physics, Russian Academy of Sciences, 142432 Chernogolovka, Russia*
[6]*Research Institute for Interdisciplinary Science, Okayama University, Okayama 700-8530, Japan*
[7]*Walther-Meissner-Institut, Bayerische Akademie der Wissenschaften, Walther-Meissner-Strasse 8, Garching D-85748, Germany*
[8]*Department of Physics and Center for Functional Materials, Wake Forest University, Winston-Salem, North Carolina 27109, USA*

(Received 14 June 2021; accepted 25 August 2021; published 29 September 2021)

Organic salts represent an ideal experimental playground for studying the interplay between magnetic and charge degrees of freedom, which has culminated in the discovery of several spin-liquid candidates such as $\kappa$-$(ET)_2Cu_2(CN)_3$ ($\kappa$-Cu). Recent theoretical studies indicate the possibility of chiral spin liquids stabilized by ring exchange, but the parent states with chiral magnetic order have not been observed in this material family. In this Letter, we discuss the properties of the recently synthesized $\kappa$-$(BETS)_2Mn[N(CN)_2]_3$ ($\kappa$-Mn). Based on analysis of specific heat, magnetic torque, and NMR measurements combined with *ab initio* calculations, we identify a spin-vortex crystal order. These observations definitively confirm the importance of ring exchange in these materials and support the proposed chiral spin-liquid scenario for triangular lattice organics.

DOI: 10.1103/PhysRevLett.127.147204

*Introduction.*—The role of higher order magnetic couplings in organic quantum spin-liquid (QSL) candidates such as $\kappa$-$(ET)_2Cu_2(CN)_3$ ($\kappa$-Cu) has been well discussed over the past two decades [1–5]. These materials are Mott insulators but exist on the verge of itinerancy, such that conventional nearest neighbor magnetic couplings are insufficient. Instead, one must consider higher order terms such as four-spin ring-exchange $K_{ijkl}(\mathbf{S}_i \cdot \mathbf{S}_j)(\mathbf{S}_k \cdot \mathbf{S}_l)$. These interactions are thought to play a crucial role in promoting a QSL ground state [1,3,4]. In general, phases characterized by scalar chiral [e.g., $\mathbf{S}_i \cdot (\mathbf{S}_j \times \mathbf{S}_k)$] and/or vector chiral (e.g., $\sum \mathbf{S}_i \times \mathbf{S}_j$) order parameters tend to be selected by large ring exchange. These include additional ordered phases in classical ring-exchange models [6–16]. Additionally, a flurry of recent proposals [17–21] have identified a chiral spin liquid (CSL) derived from these classical orders as a leading candidate for the ground state of $\kappa$-Cu. Thus, if $\kappa$-Cu is indeed a CSL, then the related chiral magnetic orders (predicted to persist away from the CSL) should also be observable in other organic materials with suitably tuned couplings.

In this Letter, we consider the magnetic ground state of $\kappa$-$(BETS)_2Mn[N(CN)_2]_3$ ($\kappa$-Mn) [22–30]. This material has a layered structure (Fig. 1) typical of $\kappa$-phase materials [31]. The organic layer is composed of $[BETS]_2^{1+}$(=bisethylenedithio-tetraselenafulvalene) dimers forming a distorted triangular lattice with $S = 1/2$ per dimer. The anion layer is composed of Mn(II) ($S = 5/2$) ions also forming a distorted triangular lattice, linked by dicyanamide bridges. The phase diagram of $\kappa$-Mn [25] is similar to $\kappa$-phase ET salts such as the spin-liquid candidate $\kappa$-Cu [32,33] and the antiferromagnet $\kappa$-$(ET)_2Cu[N(CN)_2]_2Cl$ [34–36] ($\kappa$-Cl). All have insulating ground states at low pressure, which are suppressed in favor of metallicity and superconductivity under mild pressure.

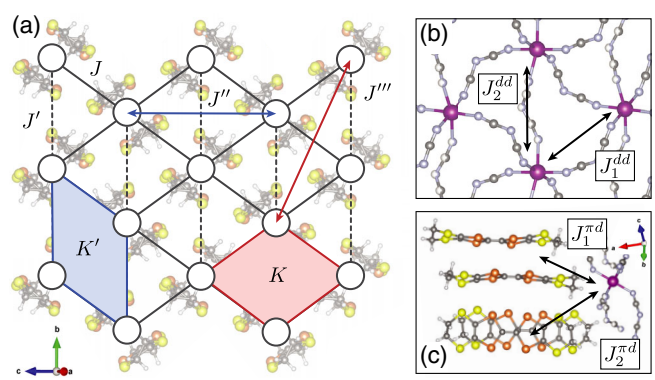


FIG. 1. Definition of (a) $\pi$-$\pi$ couplings between $S = \frac{1}{2}$ BETS dimers in the organic layer of $\kappa$-Mn. (b) $d$-$d$ couplings between $S = \frac{5}{2}$ Mn(II) in the anion layer. (c) $\pi$-$d$ couplings between BETS and Mn. $J$ labels two-spin interactions, while $K$ labels four-spin interactions.

 © 2021 American Physical Society

At elevated temperatures, the electrical conductivity of $\kappa$-Mn decreases with increasing temperature, typical of a metallic state. Magnetic order in the BETS layer onsets at $T_N \sim 22$ K in conjunction with a metal-insulator transition (MIT). This transition is marked by a significant broadening of the $^{13}$C NMR resonances [27,28] and the appearance of a field-induced spin reorientation detected via magnetic torque [26,29]. However, as we elaborate in this Letter, the angle dependence of the torque and specific pattern of NMR resonances are incompatible with conventional collinear magnetic orders. The precise magnetic structure and the role of Mn spins remain open questions [26,29].

To address these questions, we first present *ab initio* calculations and specific heat measurements that indicate negligible coupling between the BETS and Mn spins. We then establish the minimal magnetic model for the BETS layers and show that the ring exchange is sufficient to induce four-sublattice chiral order analogous to the spin-vortex crystal (SVC) observed in some Fe-based superconductors [37–40] and other models [41,42]. Finally, we show that the $^{13}$C NMR [27,28] and magnetic torque [26,29] experiments are compatible only with this chiral order, thus providing the first direct proof for the importance of ring exchange in these materials.

*Role of Mn spins.*—The magnetic couplings (Fig. 1) can be divided into three categories: $\pi$-$\pi$ (between BETS dimers), $d$-$d$ (between Mn ions), and $\pi$-$d$ (between Mn and BETS). The latter two can be summarized as

$$\mathcal{H}^{\pi d} + \mathcal{H}^{dd} = \sum_{\text{in}} J_{ij}^{\pi d} \mathbf{s}_i \cdot \mathbf{S}_n + \sum_{nm} J_{nm}^{dd} \mathbf{S}_n \cdot \mathbf{S}_m, \quad (1)$$

where $\mathbf{s}_i$ is a BETS spin ($S = 1/2$) at site $i$ and $\mathbf{S}_n$ is a Mn spin ($S = 5/2$) at site $n$. Following the approach of [43], we have estimated $J^{dd}$ and $J^{\pi d}$ using hopping parameters obtained from density functional theory calculations. Full details are given in the Supplemental Material [44]. Within the Mn layer, there are two dominant couplings [Fig. 1(b)]; we calculate $J_1^{dd} \approx J_2^{dd} \sim 0.5$–$1.0$ K. These interactions are both frustrated and disordered due to random arrangements of the $N(CN)_2$ bridges. For the $\pi$-$d$ interactions, we also estimate a very small magnitude of $J_n^{\pi d} < 0.1$ K, which suggests the BETS and Mn are essentially decoupled. The weak $\pi$-$d$ and $d$-$d$ couplings are consistent with weak antiferromagnetic tendencies of the Mn spins (experimentally, $\Theta_{\text{Mn}} = -2\langle S^2 \rangle J^{dd} \sim -5$ K) [26]. It is therefore expected that the Mn spins remain disordered down to temperatures well below $T_N \approx 22$ K.

To assess these energy scales experimentally, we measured the specific heat of $\kappa$-Mn. Figure 2 shows the electronic and magnetic specific heat divided by temperature, $\Delta C/T$, estimated by subtracting a smooth background as a proxy for phononic contributions (see the Supplemental Material [44] for details). The peak in $\Delta C/T$ at $T_N \sim 21.5$ K signals the MIT that occurs concomitantly

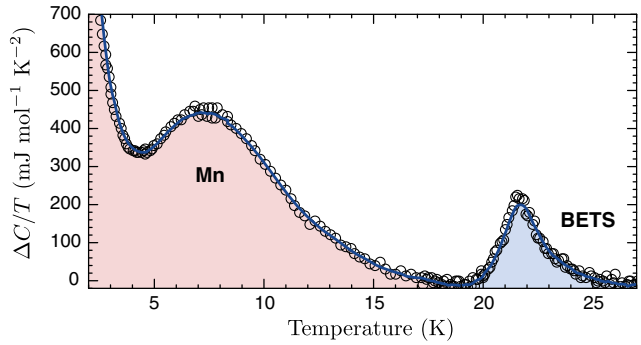


FIG. 2. Specific heat of $\kappa$-Mn after subtraction of a smooth phononic background (see the Supplemental Material [44]). The pink (blue) area indicates the estimate of entropy associated with the Mn (BETS).

with the magnetic ordering of the BETS spins. The entropy change is estimated as $\Delta S_{\text{MIT}} \approx \int_{19}^{25} \Delta C/T \, dT \approx (0.4 \pm 0.1)\ \text{J} \cdot \text{mol}^{-1} \cdot \text{K}^{-1}$ (8% of $R \ln 2$), which is too small to indicate significant participation of the Mn spins. Instead, the entropy change is comparable to $\kappa$-ET salts with nonmagnetic anions; for example, $\Delta S \approx 0.25\ \text{J} \cdot \text{mol}^{-1} \cdot \text{K}^{-1}$ was measured across the (charge-order) MIT in an ET-based salt [61], while magnetic ordering in the insulating $\kappa$-Cl was reported to have negligible $\Delta S$ [62].

For further comparison, $\Delta S_{\text{MIT}}$ is one order of magnitude larger in $\lambda - (\text{BETS})_2\text{FeX}_4$ (X = Cl, Br), where sizable $\pi - d$ interactions lead to simultaneous ordering of the $Fe^{3+}$ and $\pi$ system [43,63,64]. In these $\lambda$-phase materials, $\pi$-$d$ coupling also produces additional signatures that are absent in $\kappa$-Mn: (i) no field-induced Jaccarino-Peter superconductivity [25,26] and (ii) no beats in the Shubnikov-de Haas effect [30]. We therefore conclude that the $\pi$-$d$ coupling is sufficiently weak that the Mn spins play no significant role.

Below $T_N$, a separate broad feature in $\Delta C/T$ appears centered around 8 K, followed by a pronounced increase of $\Delta C/T$ below $\sim$4 K. Given limitations in the lowest accessible temperature, this provides only a lower bound of the associated entropy: $\Delta S_{\text{Mn}} > \int_2^{19} \Delta C/T \, dT \approx 4.4\ \text{J} \cdot \text{mol}^{-1} \cdot \text{K}^{-1}$ (29% of $R \ln 6$). This distinctly larger entropy change can be associated only with growing antiferromagnetic correlations between Mn spins. The temperature scales are compatible with the computed $J^{dd}$ couplings and measured $\Theta_{\text{Mn}}$ [26]. The multiple features in $\Delta C/T$ may reflect the combined frustration [65,66] and disorder, with the increase below 4 K potentially signifying the onset of freezing or ordering of the Mn spins.

*Magnetic model for BETS.*—Given the weak $\pi$-$d$ couplings, we focus on the $\pi$-$\pi$ couplings:

$$\mathcal{H}^{\pi\pi} = \sum_{ij} (J_{ij}^{\pi\pi} \mathbf{s}_i \cdot \mathbf{s}_j + \mathbf{D}_{ij}^{\pi\pi} \cdot \mathbf{s}_i \times \mathbf{s}_j + \mathbf{s}_i \cdot \mathbf{\Gamma}_{ij}^{\pi\pi} \cdot \mathbf{s}_j) + \frac{1}{S^2} \sum_{ijkl} K_{ijkl}^{\pi\pi} P_{ijkl} \quad (2)$$

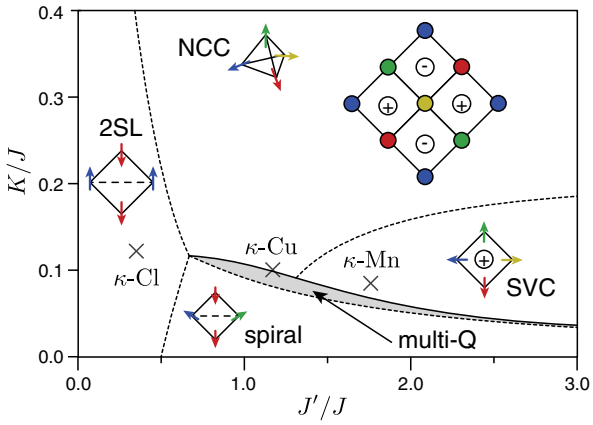


FIG. 3. Classical phase diagram for the model defined by Eq. (2), with the constraints $J'/J = J'''/J'' = K'/K$, and $K/J'' = 2$, and $|\mathbf{D}| = |\mathbf{\Gamma}| = 0$. The approximate locations of various organic materials are indicated. 2SL, two-sublattice Neel order; SVC, four-sublattice coplanar spin-vortex crystal; NCC, four-sublattice noncoplanar chiral. Dashed (solid) lines indicate transitions expected to be continuous (first order). The staggered pattern of vector chirality $\mathbf{v}_p$ for the NCC and SVC phases is indicated by $\oplus$, $\ominus$ in the inset. The locations of $\kappa$-Cu and $\kappa$-Cl are based on [67,74].

$$P_{ijkl} = [(\mathbf{s}_i \cdot \mathbf{s}_j)(\mathbf{s}_k \cdot \mathbf{s}_l) + (\mathbf{s}_j \cdot \mathbf{s}_k)(\mathbf{s}_i \cdot \mathbf{s}_l) - (\mathbf{s}_i \cdot \mathbf{s}_k)(\mathbf{s}_j \cdot \mathbf{s}_l)], \tag{3}$$

where $K^{\pi\pi}_{ijkl}$, $\mathbf{D}^{\pi\pi}_{ij}$, $\mathbf{\Gamma}^{\pi\pi}_{ij}$ parametrize the four-site ring exchange, Dzyaloshinskii-Moriya (DM) interaction, and pseudo-dipolar coupling, respectively. The unique exchange constants are defined according to Fig. 1(a). To estimate the magnitudes of the couplings, we employed the *ab initio* method outlined in [67] (see the Supplemental Material [44] for full details). The results are summarized as follows. For the isotropic couplings, we estimate $J = 260$ K, $J' = 530$ K, $J'' = 4.7$ K, $J''' = 26$ K, $K = 16$ K, and $K' = 39$ K. For the anisotropic couplings, the presence of a crystallographic inversion center ensures that $|\mathbf{D}'| = 0$ and $|\Gamma'| \approx 0$. As a result, the only significant anisotropic couplings appear for the nearest neighbor dimers, with $\mathbf{D} = (\pm 22.6, \mp 1.9, \pm 8.8)$ K oriented approximately along the long axis of the dimers. For the specific orientations of each $\mathbf{D}$ vector, see the Supplemental Material [44]. The larger magnitude of the anisotropic couplings compared to ET salts [67] is due to enhanced spin-orbit coupling afforded by the heavy Se atoms in the BETS molecules.

In Fig. 3, we show the classical phase diagram of model (2), taking the anisotropic couplings to zero and using the approximate ratios of the isotropic couplings suggested from perturbation theory [4]. Recent density matrix renormalization group studies [17,19] of the Hubbard model have found a similar quantum phase diagram, enriched by QSL states. Various regions of the phase diagram have also been studied previously [4,9–14,68,69]. The limit $J \gg J'$ corresponds to the square lattice, for which the ground state is a collinear two-sublattice (2SL) Néel order. For small $K$, this is bordered by a family of coplanar spiral states, typically with incommensurate wavevectors. This family includes, as a special case for the triangular lattice ($J'/J = 1$), conventional 120° order. Starting from this point and increasing $K$ leads first to a narrow multi- $Q$ state with a modulated canting of spins out of the plane of the spiral [13]. For larger $K$, there is a noncoplanar chiral (NCC) phase. The spin orientation in the NCC phase can be understood as follows: starting from the 2SL state with spins oriented perpendicular to the plane, each spin is then canted toward the plane to form four sublattices in the pattern indicated in Fig. 3. For the special case $J'/J = 1$, spins on different sublattices satisfy $\mathbf{s}_i \cdot \mathbf{s}_j = -S^2/3$, as if oriented along the vertices of a tetrahedron [11–13]. With increasing $J'$, the spins completely tilt toward a common plane, leading to the coplanar spin-vortex crystal (SVC) [10,14]. $\kappa$-Mn differs from other organics primarily in terms of $J'/J \approx (t'/t)^2$, which has been estimated as ~0.2–0.35 for $\kappa$-Cl [67,70–72], ~0.8–1.2 for $\kappa$-Cu [67,70,71,73], and ~2 for $\kappa$-Mn. Based on the computed couplings, the classical ground state for $\kappa$-Mn is the four-sublattice SVC.

*Order parameter.*—The SVC and NCC phases are distinguished by a finite vector chiral order parameter. Specifically, for each four-site square plaquette $p$ defined by the $J$ bonds [solid lines, Fig. 1(a)], we define a vector chirality $\mathbf{v}_p = \mathbf{s}_1 \times \mathbf{s}_2 + \mathbf{s}_2 \times \mathbf{s}_3 + \mathbf{s}_3 \times \mathbf{s}_4 + \mathbf{s}_4 \times \mathbf{s}_1$. The SVC and NCC phases correspond to a staggered pattern of neighboring $\mathbf{v}_p$ vectors, depicted by $\oplus$, $\ominus$ in the inset of Fig. 3. To see why large $K$ favors finite $|\mathbf{v}_p|$, it is useful to write, for a given plaquette

$$|\mathbf{v}_p|^2 = \frac{3}{2} + \sum_{i \in \{1..4\}} \mathbf{s}_i \cdot \mathbf{s}_{i+2} - \frac{1}{2}\mathbf{s}_i \cdot \mathbf{s}_{i+1} - 2[P_{1234} - (\mathbf{s}_1 \cdot \mathbf{s}_3)(\mathbf{s}_2 \cdot \mathbf{s}_4)]. \tag{4}$$

In general, the ring exchange $K$ and couplings $J', J'''$ are minimized when nearest neighbor spins are orthogonal $\langle \mathbf{s}_i \cdot \mathbf{s}_{i+1} \rangle \sim 0$, but second neighbor spins are antiparallel ($\langle \mathbf{s}_i \cdot \mathbf{s}_{i+2} \rangle > 0, \langle P_{ijkl} \rangle < 0$), which corresponds to a finite value of $|\mathbf{v}_p|$. The 2SL and spiral phases have $|\mathbf{v}_p| = 0$.

Because of the specific symmetries of the crystal, states with finite $|\mathbf{v}_p|$ can be distinguished based on their magnetic anisotropy. Importantly, the periodicities of the DM-vector components in the $b$ and $(a^*, c)$ directions are different by symmetry (see the Supplemental Material [44]). The vector chirality couples linearly only to $\mathbf{D}_b$, which pins $\mathbf{v}_p || b$ at low fields. For the coplanar SVC phase, this confines the spins to lie in the $a^*c$ plane. In contrast, the symmetries of the 2SL and spiral phases are such that they couple only to $\mathbf{D}_{ac}$. At low fields, the energy is minimized for spins confined to the plane perpendicular to

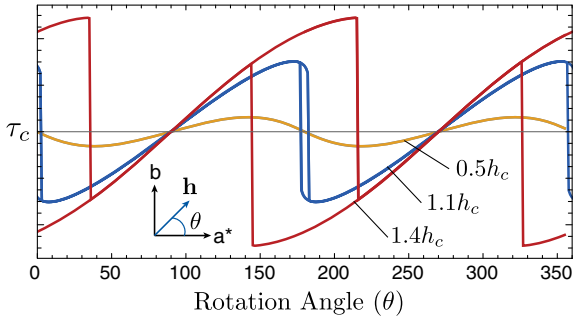


FIG. 4. Magnetic torque $dE_{\mathrm{SVC}}/d\theta$ as a function of rotation angle $\theta$ around the $c$ axis for $E_{\mathrm{SVC}}$ defined by Eq. (5). $h_c$ is the **v**-flop field at $\theta = 0$.

$\mathbf{D}_{ac}$. This distinction may be probed by the angular dependence of the magnetic torque $\tau(H,\theta)$.

*Magnetic torque.*—Although detailed analysis of recently reported $\tau(H,\theta)$ [26,29] is complicated by a background contribution from the paramagnetic Mn, we can make general observations. For $T < T_N$, steplike features appear in $\tau(H)$ due to a field-induced reorientation of ordered spins within the BETS layer. However, the torque on the BETS spins vanishes for fields oriented in the entire $a^*c$ plane. This is anomalous for two reasons: (i) for a conventional spin-flop of an easy-axis 2SL state, $\tau(H)$ vanishes by symmetry only for fields along the easy axis, rather than an entire plane, and (ii) for the 2SL (and spiral) phases, the $a^*c$ plane is not a special plane of symmetry. Taken together, these findings suggest the field couples to an order parameter of novel symmetry. Similar effects have also been seen in the related mixed Co-Mn salt [75].

These findings are consistent with an ordered phase with finite $|\mathbf{v}_p|$. By symmetry (see the Supplemental Material [44]), the free energy can be written schematically as

$$E_{\mathrm{SVC}} = -(0, d_b, 0)\cdot\mathbf{v} - (\mathbf{h}\cdot\mathbf{v})^2 + \mathcal{O}(h^4), \qquad (5)$$

where **v** is the staggered vector chirality, $d_b$ is a reduced DM coupling, and **h** is a reduced external field. The DM interaction pins $\mathbf{v}||b$ at low fields. An applied field tends to tilt the ordering plane to be perpendicular to the field. For fields oriented close the $a^*c$ plane, $d_b$ competes with the field, leading to a rapid rotation of the ordering plane at a critical field $h_c$. Such a transition may be viewed as a flop of the vector chirality. The associated torque ($\tau_c = dE_{\mathrm{SVC}}/d\theta$) for rotation around the $c$ axis is shown in Fig. 4. For $h > h_c$ there are two metastable domains with **v** tilted toward and away from **h**. This leads to widening hysteresis with increasing field, which may be related to the reported irreversibility of $\tau_c$ for field sweeps with $h > h_c$. At all fields, the average value of $\tau_c$ for $\mathbf{h}||a^*$ vanishes. Similarly, for rotation around the $b$ axis, the associated torque $\tau_b = 0$ for all field orientations.

$^{13}$C *NMR.*—As a more selective probe of the magnetic order in the BETS layer, we also consider the $^{13}$C NMR data reported in Refs. [27,28]. Below $T_N$, the resonance frequency of each $^{13}$C nucleus $n$ at dimer site $i$ shifts by $\Delta\nu_{n,i}$ from the natural Larmor frequency due to the hyperfine coupling with the local spin moment:

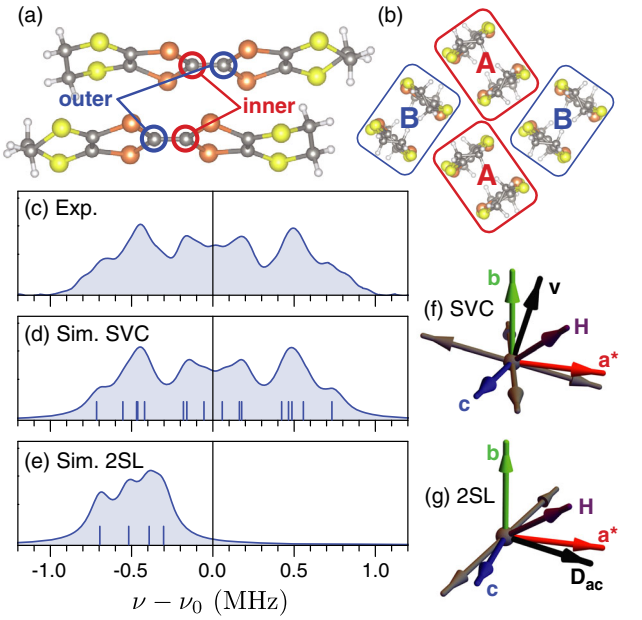


FIG. 5. (a) Distinct $^{13}$C sites in each BETS dimer. (b) Dimer sublattices. (c) Experimental $^{13}$C NMR spectra measured at 5 K and 7 T for field oriented 45° from the $a^*$ axis, and $\perp[0\bar{1}1]$ obtained from [27]. (d),(e) Simulated spectra for SVC and 2SL phases (see text). Sticks indicate resonance positions. (f),(g) Orientations of the sublattice moments (gray) for the simulations.

$$\Delta\nu_{n,i} = \gamma_C(|\mathbf{H}_{\mathrm{eff},n,i}| - |\mathbf{H}_{\mathrm{ext}}|) \qquad (6)$$

$$\mathbf{H}_{\mathrm{eff},n,i} = \mathbf{H}_{\mathrm{ext}} + \mathbb{A}_{i,n}\cdot\langle\mathbf{s}_i\rangle, \qquad (7)$$

where $\gamma_C = 10.7084$ MHz/T is the gyromagnetic ratio, $\langle\mathbf{s}_i\rangle$ is the local spin expectation value, and $\mathbb{A}_{i,n}$ is the local hyperfine coupling tensor. There are two types of isotopically enriched $^{13}$C sites per dimer, depicted in Fig. 5(a). In addition, as shown in Fig. 5(b), there are two symmetry-related dimers per unit cell (sublattices A and B). Together, this yields four crystallographically distinct $^{13}$C sites per unit cell. In Fig. 5(c), we show the experimental spectra for $T = 5$ K, and $H = 7$ T, reproduced from Ref. [27]. The field is oriented 45° from the $a^*$ axis and perpendicular to the $[0\bar{1}1]$ direction. The resonance is symmetrical about the Larmor frequency, with a rich fine structure, indicating many magnetically inequivalent $^{13}$C sites. To analyze the reported spectra, we first estimated the $\mathbb{A}$ tensors using ORCA [76] (see the Supplemental Material [44] for details). We then simulated the expected resonance patterns for different magnetic configurations, employing a Lorentzian broadening consistent with the experimental widths and ignoring the Mn dipolar fields.

From the symmetry of the resonances, the 2SL phase can be immediately ruled out. In $\kappa$-phase organics, the $A$ and $B$ dimers in the unit cell correspond precisely with the two magnetic sublattices in the 2SL state. At moderate fields, the DM interaction $\mathbf{D}_{ac}$ selects a unique preferred orientation of the sublattice moments with respect to the canted moment, leading to a single domain. As a result, the magnetically inequivalent $^{13}$C sites are in 1:1 correspondence with the crystallographically distinct sites. This leads to four distinct resonances, with asymmetrical shifts for most field directions. This property was previously employed to confirm 2SL order in $\kappa$-Cl [77]. In Fig. 5(e) we show a representative spectrum for $\kappa$-Mn in the 2SL phase, assuming the sublattice moments are oriented along $\pm\mathbf{D}_{a^*c} \times \mathbf{H}$, as shown in Fig. 5(g). The simulated spectrum is completely incompatible with the experiment.

In the SVC state, there is no unique correspondence between the crystallographic and magnetic sublattices; domains are expected in which the $A$ and $B$ sublattices are populated with spins of all four orientations. In total, this leads to 16 distinct resonances for general field orientations. The magnetic structure is symmetric under the combination of inversion and time reversal, which ensures that the NMR resonances are symmetrically distributed. To evaluate whether the experimental spectra is compatible with SVC, we fit the data for a four–magnetic sublattice model using the computed $\mathbb{A}$ tensors, constraining only $\mathbf{s}_1 = -\mathbf{s}_2$ and $\mathbf{s}_3 = -\mathbf{s}_4$. The resulting best fit [Fig. 5(d)] shows almost perfect agreement with the experiment. The fitted ordered moment is only $\langle \mathbf{s}_i \rangle = 0.15\ \mu_B$, which suggests strong quantum and/or thermal fluctuations. More importantly, the orientations of the fitted moments [Fig. 5(f)] conform with the expectations for SVC. The fitted moments are nearly orthogonal, and the vector chirality $\mathbf{v}$ is oriented close to the $b$ axis, but tilted toward the external field $\mathbf{H}$.

*Discussion.*—On this basis, we conclude the anomalous $^{13}$C NMR and magnetic torque response are both consistent with SVC order in $\kappa$-Mn, which is stabilized by higher order interactions including ring exchange. This serves as definitive proof of the relative importance of such terms and establishes $K/J \sim 0.1$. While the role of disorder has also been recently discussed for $\kappa$-Cu [74,78], the possibility of a (gapped) CSL state [17–21] should be considered seriously, given that the parent chiral ordered state has now been observed in $\kappa$-Mn.

We acknowledge useful discussions with Y. Agarmani. S. M. W. acknowledges support through an NSERC Canada Postdoctoral Fellowship. K. R., M. L., and R. V. acknowledge support by the Deutsche Forschungsgemeinschaft (DFG, German Research Foundation) for funding through TRR 288–422213477 (Project No. A05 and No. A06). O. M. V., N. D. K., and M. V. K. acknowledge financial support from the German Research Foundation (Deutsche Forschungsgemeinschaft, DFG) via Grant No. KA 1652/5-1 and from the Russian Foundation for Basic Research, Grant No. 21-52-12O27. N. D. K. also acknowledges the support of the State Assignment of the topic No. AAAA-A19-11902390079-8.

*winters@wfu.edu

[1] O. I. Motrunich, Phys. Rev. B **72**, 045105 (2005).
[2] S.-S. Lee and P. A. Lee, Phys. Rev. Lett. **95**, 036403 (2005).
[3] M. S. Block, D. N. Sheng, O. I. Motrunich, and M. P. A. Fisher, Phys. Rev. Lett. **106**, 157202 (2011).
[4] M. Holt, B. J. Powell, and J. Merino, Phys. Rev. B **89**, 174415 (2014).
[5] Y. Zhou, K. Kanoda, and T.-K. Ng, Rev. Mod. Phys. **89**, 025003 (2017).
[6] M. Roger, J. M. Delrieu, and J. H. Hetherington, Phys. Rev. Lett. **45**, 137 (1980).
[7] M. Roger, J. H. Hetherington, and J. M. Delrieu, Rev. Mod. Phys. **55**, 1 (1983).
[8] M. Roger and J. H. Hetherington, Phys. Rev. B **41**, 200 (1990).
[9] M. Roger and J. M. Delrieu, Phys. Rev. B **39**, 2299 (1989).
[10] A. Chubukov, E. Gagliano, and C. Balseiro, Phys. Rev. B **45**, 7889 (1992).
[11] K. Kubo and T. Momoi, Z. Phys. B **103**, 485 (1997).
[12] K. Kubo, H. Sakamoto, T. Momoi, and K. Niki, J. Low Temp. Phys. **111**, 583 (1998).
[13] K. Kubo and T. Momoi, Physica B Condens. **329–333**, 142 (2003).
[14] A. Läuchli, J. C. Domenge, C. Lhuillier, P. Sindzingre, and M. Troyer, Phys. Rev. Lett. **95**, 137206 (2005).
[15] S. Hayami, R. Ozawa, and Y. Motome, Phys. Rev. B **95**, 224424 (2017).
[16] S. Paul, S. Haldar, S. von Malottki, and S. Heinze, Nat. Commun. **11**, 4756 (2020).
[17] A. Szasz, J. Motruk, M. P. Zaletel, and J. E. Moore, Phys. Rev. X **10**, 021042 (2020).
[18] B.-B. Chen, Z. Chen, S.-S. Gong, D. Sheng, W. Li, and A. Weichselbaum, arXiv:2102.05560.
[19] A. Szasz and J. Motruk, Phys. Rev. B **103**, 235132 (2021).
[20] A. Wietek, R. Rossi, F. Šimkovic IV, M. Klett, P. Hansmann, M. Ferrero, E. M. Stoudenmire, T. Schäfer, and A. Georges, arXiv:2102.12904 [Phys. Rev. X (to be published)].
[21] T. Cookmeyer, J. Motruk, and J. E. Moore, Phys. Rev. Lett. **127**, 087201 (2021).
[22] N. D. Kushch, A. V. Kazakova, A. D. Dubrovskii, G. V. Shilov, L. I. Buravov, R. B. Morgunov, E. V. Kurganova, Y. Tanimoto, and E. B. Yagubskii, J. Mater. Chem. **17**, 4407 (2007).
[23] N. D. Kushch, E. B. Yagubskii, M. V. Kartsovnik, L. I. Buravov, A. D. Dubrovskii, A. N. Chekhlov, and W. Biberacher, J. Am. Chem. Soc. **130**, 7238 (2008).
[24] R. Morgunov, E. Kurganova, Y. Tanimoto, A. Markosyan, A. Kazakova, N. Kushch, É. Yagubskii, A. Dubrovskii, and G. Shilov, Phys. Solid State **49**, 905 (2007).
[25] V. N. Zverev, M. V. Kartsovnik, W. Biberacher, S. S. Khasanov, R. P. Shibaeva, L. Ouahab, L. Toupet, N. D. Kushch, E. B. Yagubskii, and E. Canadell, Phys. Rev. B **82**, 155123 (2010).

[26] O. M. Vyaselev, M. V. Kartsovnik, W. Biberacher, L. V. Zorina, N. D. Kushch, and E. B. Yagubskii, Phys. Rev. B **83**, 094425 (2011).

[27] O. M. Vyaselev, R. Kato, H. M. Yamamoto, M. Kobayashi, L. V. Zorina, S. V. Simonov, N. D. Kushch, and E. B. Yagubskii, Crystals **2**, 224 (2012).

[28] O. Vyaselev, M. Kartsovnik, N. Kushch, and E. Yagubskii, JETP Lett. **95**, 565 (2012).

[29] O. M. Vyaselev, W. Biberacher, N. D. Kushch, and M. V. Kartsovnik, Phys. Rev. B **96**, 205154 (2017).

[30] V. N. Zverev, W. Biberacher, S. Oberbauer, I. Sheikin, P. Alemany, E. Canadell, and M. V. Kartsovnik, Phys. Rev. B **99**, 125136 (2019).

[31] N. Toyota, M. Lang, and J. Mller, *Low-Dimensional Molecular Metals* (Springer-Verlag, Berlin, Heidelberg, 2007).

[32] Y. Kurosaki, Y. Shimizu, K. Miyagawa, K. Kanoda, and G. Saito, Phys. Rev. Lett. **95**, 177001 (2005).

[33] A. Pustogow, M. Bories, A. Lhle, R. Rsslhuber, E. Zhukova, B. Gorshunov, S. Tomi, J. A. Schlueter, R. Hbner, T. Hiramatsu, Y. Yoshida, G. Saito, R. Kato, T.-H. Lee, V. Dobrosavljevi, S. Fratini, and M. Dressel, Nat. Mater. **17**, 773 (2018).

[34] S. Lefebvre, P. Wzietek, S. Brown, C. Bourbonnais, D. Jérome, C. Mézière, M. Fourmigué, and P. Batail, Phys. Rev. Lett. **85**, 5420 (2000).

[35] P. Limelette, P. Wzietek, S. Florens, A. Georges, T. A. Costi, C. Pasquier, D. Jérome, C. Mézière, and P. Batail, Phys. Rev. Lett. **91**, 016401 (2003).

[36] E. Gati, M. Garst, R. S. Manna, U. Tutsch, B. Wolf, L. Bartosch, H. Schubert, T. Sasaki, J. A. Schlueter, and M. Lang, Sci. Adv. **2**, e1601646 (2016).

[37] J. Lorenzana, G. Seibold, C. Ortix, and M. Grilli, Phys. Rev. Lett. **101**, 186402 (2008).

[38] R. M. Fernandes, S. A. Kivelson, and E. Berg, Phys. Rev. B **93**, 014511 (2016).

[39] J. Allred, K. Taddei, D. Bugaris, M. Krogstad, S. Lapidus, D. Chung, H. Claus, M. Kanatzidis, D. Brown, J. Kang *et al.*, Nat. Phys. **12**, 493 (2016).

[40] W. R. Meier, Q.-P. Ding, A. Kreyssig, S. L. Budko, A. Sapkota, K. Kothapalli, V. Borisov, R. Valentí, C. D. Batista, P. P. Orth *et al.*, npj Quantum Mater. **3**, 5 (2018).

[41] S. Hayami and Y. Motome, Phys. Rev. B **90**, 060402(R) (2014).

[42] O. I. Utesov, Phys. Rev. B **103**, 064414 (2021).

[43] T. Mori and M. Katsuhara, J. Phys. Soc. Jpn. **71**, 826 (2002).

[44] See Supplemental Material at http://link.aps.org/supplemental/10.1103/PhysRevLett.127.147204 for detailed descriptions of the *ab initio* calculations for the magnetic couplings and NMR hyperfine tensors, as well as details of the background subtraction for the specific heat measurements, which includes Refs. [45–60].

[45] K. Koepernik and H. Eschrig, Phys. Rev. B **59**, 1743 (1999).

[46] J. P. Perdew, K. Burke, and M. Ernzerhof, Phys. Rev. Lett. **77**, 3865 (1996).

[47] H. Eschrig and K. Koepernik, Phys. Rev. B **80**, 104503 (2009).

[48] K. Nakamura, Y. Yoshimoto, and M. Imada, Phys. Rev. B **86**, 205117 (2012).

[49] D. Guterding, R. Valentí, and H. O. Jeschke, Phys. Rev. B **92**, 081109(R) (2015).

[50] H. Mayaffre, P. Wzietek, C. Lenoir, D. Jérome, and P. Batail, Europhys. Lett. **28**, 205 (1994).

[51] S. M. De Soto, C. P. Slichter, A. M. Kini, H. H. Wang, U. Geiser, and J. M. Williams, Phys. Rev. B **52**, 10364 (1995).

[52] Y. Saito and A. Kawamoto, Solid State Nucl. Magn. Reson. **73**, 22 (2016).

[53] J. Müller, M. Lang, R. Helfrich, F. Steglich, and T. Sasaki, Phys. Rev. B **65**, 140509(R) (2002).

[54] Y. Nakazawa and K. Kanoda, Phys. Rev. B **53**, R8875 (1996).

[55] R. Świetlik, H. Grimm, D. Schweitzer, and H. J. Keller, Z. Naturforsch. A **42**, 603 (1987).

[56] J. Wosnitza, X. Liu, D. Schweitzer, and H. J. Keller, Phys. Rev. B **50**, 12747 (1994).

[57] S. Katsumoto, S.-i. Kobayashi, H. Urayama, H. Yamochi, and G. Saito, J. Phys. Soc. Jpn. **57**, 3672 (1988).

[58] B. Andraka, J. S. Kim, G. R. Stewart, K. D. Carlson, H. H. Wang, and J. M. Williams, Phys. Rev. B **40**, 11345 (1989).

[59] G. R. Stewart, J. O'Rourke, G. W. Crabtree, K. D. Carlson, H. H. Wang, J. M. Williams, F. Gross, and K. Andres, Phys. Rev. B **33**, 2046 (1986).

[60] Y. Agarmani, T. Thomas, S. Hartmann, M. Kartsovnik, N. Kushch, S. M. Winter, M. Lang, and J. Müller (to be published).

[61] E. Gati, J. K. H. Fischer, P. Lunkenheimer, D. Zielke, S. Köhler, F. Kolb, H. A. K. von Nidda, S. M. Winter, H. Schubert, J. A. Schlueter, H. O. Jeschke, R. Valentí, and M. Lang, Phys. Rev. Lett. **120**, 247601 (2018).

[62] S. Yamashita and Y. Nakazawa, J. Therm. Anal. Calorim. **99**, 153 (2010).

[63] T. Konoike, S. Uji, T. Terashima, M. Nishimura, S. Yasuzuka, K. Enomoto, H. Fujiwara, B. Zhang, and H. Kobayashi, Phys. Rev. B **70**, 094514 (2004).

[64] M. V. Kartsovnik, M. Kunz, L. Schaidhammer, F. Kollmannsberger, W. Biberacher, N. D. Kushch, A. Miyazaki, and H. Fujiwara, J. Supercond. Novel Magn. **29**, 3075 (2016).

[65] B. Schmidt and P. Thalmeier, New J. Phys. **17**, 073025 (2015).

[66] U. Tutsch, O. Tsyplyatyev, M. Kuhnt, L. Postulka, B. Wolf, P. T. Cong, F. Ritter, C. Krellner, W. Aßmus, B. Schmidt, P. Thalmeier, P. Kopietz, and M. Lang, Phys. Rev. Lett. **123**, 147202 (2019).

[67] S. M. Winter, K. Riedl, and R. Valentí, Phys. Rev. B **95**, 060404(R) (2017).

[68] C. Yasuda, Y. Uchihira, S. Taira, and K. Kubo, J. Phys. Soc. Jpn. **87**, 104704 (2018).

[69] L. Messio, C. Lhuillier, and G. Misguich, Phys. Rev. B **83**, 184401 (2011).

[70] H. C. Kandpal, I. Opahle, Y.-Z. Zhang, H. O. Jeschke, and R. Valentí, Phys. Rev. Lett. **103**, 067004 (2009).

[71] K. Nakamura, Y. Yoshimoto, T. Kosugi, R. Arita, and M. Imada, J. Phys. Soc. Jpn. **78**, 083710 (2009).

[72] A. C. Jacko, E. P. Kenny, and B. J. Powell, Phys. Rev. B **101**, 125110 (2020).

[73] T. Koretsune and C. Hotta, Phys. Rev. B **89**, 045102 (2014).

[74] K. Riedl, R. Valentí, and S. M. Winter, Nat. Commun. **10**, 2561 (2019).

[75] N. D. Kushch, O. M. Vyaselev, V. N. Zverev, W. Biberacher, L. I. Buravov, E. B. Yagubskii, E. Herdtweck, E. Canadell, and M. V. Kartsovnik, Synth. Met. **227**, 52 (2017).

[76] F. Neese, F. Wennmohs, U. Becker, and C. Riplinger, J. Chem. Phys. **152**, 224108 (2020).

[77] K. Miyagawa, K. Kanoda, and A. Kawamoto, Chem. Rev. **104**, 5635 (2004).

[78] B. Miksch, A. Pustogow, M. J. Rahim, A. A. Bardin, K. Kanoda, J. A. Schlueter, R. Hübner, M. Scheffler, and M. Dressel, Science **372**, 276 (2021).